Check for updates

Received: 14 November 2019 | Revised: 26 February 2020 | Accepted: 28 March 2020

DOI: 10.1111/grs.12288

ORIGINAL ARTICLE

GRASSLAND SCIENCE | WILEY

Discriminating *Pennisetum alopecuoides* plants in a grazed pasture from unmanned aerial vehicles using object-based image analysis and random forest classifier

Norio Yuba[1,2] | Kensuke Kawamura[3] | Taisuke Yasuda[4] | Jihyun Lim[5] | Rena Yoshitoshi[6] | Nariyasu Watanabe[6] | Yuzo Kurokawa[7] | Teruo Maeda[7]

[1]Graduate School for International Development and Cooperation (IDEC), Hiroshima University, Higashi-Hiroshima, Japan

[2]Forestry Research Center, Hiroshima Prefectural Technology Research Institute, Higashi-Hiroshima, Japan

[3]Japan International Research Center for Agricultural Sciences (JIRCAS), Tsukuba, Japan

[4]Mount Fuji Research Institute, Yamanashi Prefectural Government, Fujiyoshida, Japan

[5]Research Center for Agricultural Information Technology, National Agriculture and Food Research Organization (NARO), Tsukuba, Japan

[6]Western Region Agricultural Research Center, National Agriculture and Food Research Organization (NARO), Oda, Japan

[7]Graduate School of Integrated Sciences for Life, Hiroshima University, Higashi-Hiroshima, Japan

Correspondence
Kensuke Kawamura, Japan International Research Center for Agricultural Sciences, 1-1 Ohwashi, Tsukuba, Ibaraki 305-8686, Japan.
Email: kamuken@affrc.go.jp

Abstract

Timely and accurate weed detection in pasture is critical for efficient grazing management. Although high-resolution images from unmanned aerial vehicles (UAVs) offer new opportunities for the detection of weeds at the farm scale, pixel-based image analyses do not always produce the best results and object-based image analysis (OBIA) has improved weed discrimination accuracy. In the present study, we evaluated the performance of OBIA on UAV images by integrating random forest (RF) classifier with auxiliary information layers to discriminate and map *Pennisetum alopecuroide* plants, a prolific and harmful weed, in a grazed pasture. The UAV images were captured at different flight altitudes (28, 56, 82 and 114 m). The OBIA-RF algorithm included 20 input features: five layers (red-green-blue [RGB] or hue-saturation-brightness [HSV] image bands, texture and digital surface model) and the descriptive statistics (median, standard deviation, minimum and maximum) for each object. The predicted *P. alopecuroides* maps were evaluated for out-of-bag accuracy and generalized error accuracy in the test dataset. HSV-based classification had higher classification accuracy, and the lowest altitude of 28 m (spatial resolution, 0.9 cm) was considered the most suitable for the weed detection. Overall, the optimal classification accuracy was achieved in the HSV-based OBIA-RF model using the images from the lowest altitude (highest spatial resolution). Among the 20 input features, the brightness information (V layer) in the HSV images was considered the most important because *P. alopecuroides* ears are black.

KEYWORDS

grazing management, machine learning, unmanned aerial vehicle, weed detection

1 | INTRODUCTION

Timely and accurate detection of weed invasions in a pasture is critical in grazing management. Weed invasion and dominance in a pasture reduces the grazing capacity. Therefore, to estimate grazing capacity accurately, it is necessary to establish the weed cover in a pasture. Recently, unmanned aerial vehicle (UAV)-based low-altitude remote sensing technologies have become promising tools for weed management. In general, weeds occur in patches rather than uniformly across fields; however, conventional management practices rely on whole-field management (Ghanizadeh & Harrington, 2019; Llewellyn, Lindner, Pannell, & Powles, 2004). Site-specific weed management has considerable potential economic and environmental benefits (Shaw, 2005).

With the increasing accessibility of very-fine-resolution UAV imagery, optimum spatial resolution has been explored in weed

 © 2020 Japanese Society of Grassland Science

mapping (Gebhardt & Kühbauch, 2007; Tamouridou et al., 2017). While mapping the early stages of broadleaved weeds, spatial resolution at 2-cm spatial resolution exhibited higher performance than 4-cm spatial resolution (Peña, Torres-Sánchez, Serrano-Pérez, de Castro, & López-Granados, 2015). However, the highest resolutions did not always yield the best results, and a "salt and pepper" effect would be discernible in the classification results. In our previous study (Yuba et al., 2020), we considered that *Pennisetum alopecuroides* (L.) Spreng ears are black and developed a simple algorithm based on a pixel-based computer vision technique to count the number of *P. alopecuroides* plants from UAV images at different flight altitudes. According to the results, the second highest spatial resolution image data (1.82 cm) yielded results superior to the ones obtained from the highest spatial resolution image data (0.90 cm).

Unlike pixel-based classification, object-based image analysis (OBIA) data represents the spatial neighborhood properties rather than single pixels. OBIA is an image-processing approach that treats adjacent pixels as objects, taking into consideration parameters such as object shape and homogeneity, in addition to the spectral information. Because weeds tend to grow into patches, OBIA has been applied in weed mapping using UAV images (Blaschke et al., 2014). OBIA techniques can be used to classify challenging scenarios by combining spectral, topological and contextual information from such objects (Peña, Torres-Sánchez, de Castro, Kelly, & López-Granados, 2013).

More recently, the superpixel technique, which was introduced by Ren and Malik (2003), began to be applied extensively to high-spatial resolution image segmentation due to its ability to generate uniform and homogenous regions that preserve most of the useful information (Beaulieu & Goldberg, 1989; Tremeau & Colantoni, 2000). A superpixel refers an irregular pixel block that is visually important and consists of adjacent pixels of similar color, texture, brightness, etc. The superpixel algorithms can be classified into two major types: i) algorithms based on gradient ascent methods, such as the mean shift algorithm (Comaniciu & Meer, 2002), the watershed transform algorithm (Haris, Efstratiadis, & Maglaveras, 1998), and the simple linear iterative clustering (SLIC) algorithm (Achanta et al., 2012), and ii) algorithms based on the graph theory such as the normalized cuts algorithm (Shi & Malik, 2000) and efficient graph-based image segmentation (Felzenszwalb & Huttenlocher, 2004). Among the algorithms above, SLIC exhibits a good balance between accuracy and computational efficiency (Stutz, Hermans, & Leibe, 2018). Therefore, it has been applied extensively to high-spatial remote sensing data (Cheng, Mitra, Huang, Torr, & Hu, 2015; Csillik, 2017; Wang, Dong, Cheng, & Li, 2018).

To date, numerous classification methods have been developed and utilized to map weeds from UAV images. Particularly for high dimensional and complex data, machine learning approaches have emerged as more accurate and efficient compared to conventional parametric method (Rodriguez-Galiano, Ghimire, Rogan, Chica-Olmo, & Rigol-Sanchez, 2012). Among the numerous machine learning approaches available, the random forest (RF) classifier has increasingly attracted the attention of researchers due to its generalized performance and operation speed (Belgiu & Drăguţ, 2016; Rodriguez-Galiano et al., 2012). Classification accuracy could be enhanced by combining RF classifier with OBIA (de Castro et al., 2018). In addition, previous studies have reported that weed detection from UAV images could be improved using auxiliary information layers, such as spatial texture and vegetation height estimated from UAV digital surface models (DSM) (Zisi et al., 2018). From these earlier findings, we can expect improvement of weed detection accuracy by combining OBIA and RF classification using UAV's color images and its auxiliary information.

In the present study, we evaluated the performance of OBIA-RF algorithms in the discrimination of *P. alopecuroides* plants in a grazed pasture using UAV images at different flight altitudes. We focused on the fact that *P. alopecuroides* plants ears are black that represents black dots in image from sky and performed UAV observation at heading stage. In OBIA, we used the SLIC superpixel technique to extract the input feature information in each object, which included red-green-blue (RGB) or hue-saturation-brightness (HSV) color information, DSM and spatial texture. *P. alopecuroides*, which is a bunch-type grass and is considered a prolific harmful weed, is widely distributed in grazed pasture from the Kyushu to Hokkaido regions in Japan (Sakai, 1978). The cattle grazing preference for the species is low. In addition, the brush-like spikes stick to the hair of cattle and they are dispersed across pasture by the animals (Ide, Koyama, Takahashi, Kobayashi, & Fukuda, 2006; Sakai, 1978). Over the last three decades, efforts have been made to control *P. alopecuroides* or to exploit it as feed for grazing animals (Hayashi, 2002; Takahashi, Takahashi, Shibayama, & Imura, 1999; Takahashi & Takahashi, 1999).

2 | MATERIALS AND METHODS

2.1 | Experimental paddock and field observation

The present study used UAV images used in our previous study (Yuba et al., 2020); the UAV image data were acquired at heading stage of *P. alopecuroide* plants in 24 September 2016, from a grazed paddock (1.4 ha) at the Setouchi Field Science Center, Saijo Station, Graduate School of Biosphere Science, Hiroshima University, Japan (N34°24′, E132°43′). The area is located in a temperate zone with a warm, humid summer, and a cool, dry winter (Lim et al., 2015). The mean annual precipitation is 14.6°C, and the annual precipitation was 1960 mm in 2016. Over the last decade, the pasture has been stocked with 4–9 Japanese Black cows (*Bos taurus* L.) during the growing season from early May to late October.

In an experimental paddock, we selected areas that *P. alopecuroides* plants had severely invaded and set up two 20 m × 20 m quadrat A and B plots as illustrated in Figure 1. After the UAV flight, *P. alopecuroides* locations within the plots were recorded for the determination of ground-truth data. In addition, plant widths (diameter, cm) and plant heights (cm) of *P. alopecuroides* plants were measured within the plots (n = 811). The locations of *P. alopecuroides* and other plants (other vegetation, dead materials and soil surface) were

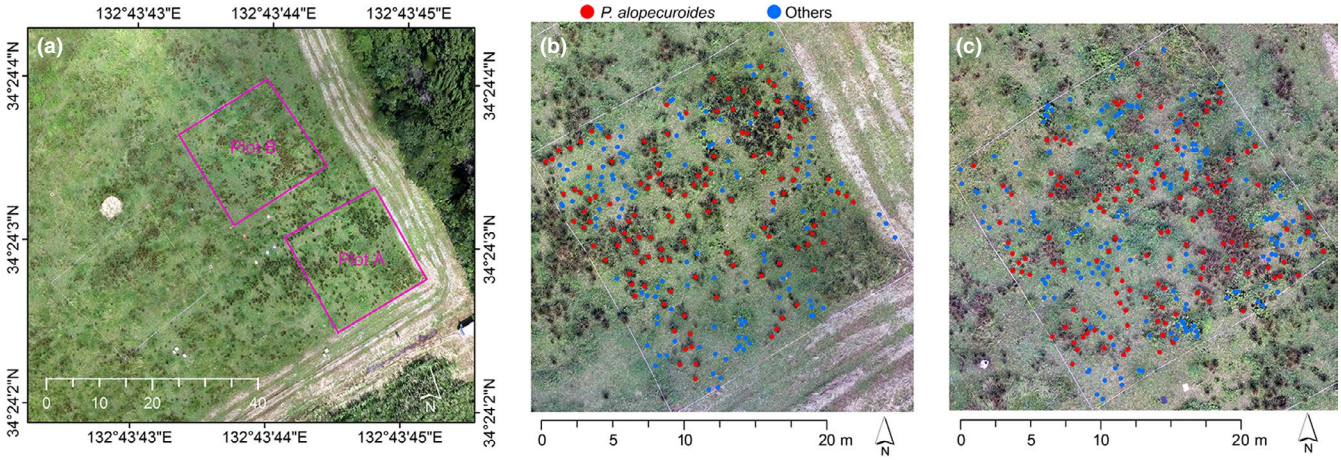

FIGURE 1 Experimental paddock and locations of two plots (a) and field observed locations of *Pennisetum alopecuroides* (red circles) and other plants (blue circles) in plot A (b) and plot B (c)

checked visually and plotted on the printed UAV images by hand in the field. Subsequently, the spatial data points in plot A (Figure 1b; n = 259 [*P. alopecuroides* = 134, others = 125]) and plot B (Figure 1c; n = 314 [178, 136]) were generated in shape file format using ArcGIS version 10.6 (ESRI).

2.2 | Overview of the methodology

In the present section, we present an overview of the research process using a flowchart (Figure 2) that summarizes five steps: (a) acquisition of UAV images, ground control points (GCP) and ground-truth data; (b) generation of dense point clouds, DSM and ortho-mosaiced RGB images; (c) generation of HSV and texture images (spatial variety of the G band) from mosaic RGB images; (d) image segmentation and calculation of four features within each segment for 5 layers (RGB or HSV + DSM + Texture); (e) calculation of RF classifier and generation of *P. alopecuroides* spatial distribution maps.

UAV image acquisition in step 1 was performed using a DJI Phantom 2 (DJI) with a commercial digital camera (PowerShot S110, Canon). Dense point cloud, DSM and RGB image generation in step 2 were performed using Agisoft Metashape Pro version 1.5.1 (Agisoft LLC). In step 3, HSV and texture images were calculated using MATLAB version 9.3 (MathWorks). Image segmentation in step 4 and image classification in step 5 were performed using Python programming language.

The OBIA-RF algorithm used in the present study was developed originally by (Yasuda, 2018) for classifying shrubs that invaded semi-natural grasslands. In the original methods, the input features include topographic openness, which expresses the dominance (positive) or enclosure (negative) of a landscape (Yokoyama, Shirasawa, & Pike, 2002). Although topographic openness would be a meaningful input feature at landscape scale for detecting trees or shrub in the grasslands, it is not suitable for weed detection within paddock scale. In the present study, we used spatial texture (Zisi et al., 2018) instead of openness.

2.3 | UAV image and GCP acquisition in field

Aerial images of the target area were acquired at different flight altitudes (28, 56, 82, and 114 m) using Canon PowerShot S100 camera mounted on a commercial UAV, DJI Phantom 2. The PowerShot S100 camera acquired 12-megapixel images in RGB color with 8-bit radiometric resolution (4,000 × 3,000 pixels, focal length 5.2 mm). UAV flight was performed by manual operation at 11:00–12:00 on 24 September 2016. Canon Hack Development Kit (http://chdk.wikia.com) was installed in the camera to trigger the camera shutter every 2 s during flight.

Five wooden boards (30 × 30 cm) were placed at the four corners and at the center position of each plot as ground control points (GCPs). A differential global positioning system (Geo7X, Trimble) was used to record the GCPs position. The GCP data gave horizontal and vertical resolutions of <15 cm after postprocessing using Trimble Pathfinder Office (Trimble).

2.4 | Dense point cloud, DSM and RGB generation

Using the commercial structure from motion (SfM) software, Metashape Pro version 1.5.1, 3D dense point clouds, DSM and ortho-mosaic RGB images were constructed from images taken by the UAV at different altitudes based on the geographic coordinates of six GCPs (UTM 53N). SfM is a computer technique that can generate 3D geometries by automatically extracting the corresponding feature points from unordered overlapped multi-view stereo UAV-based RGB images, and optimizing the 3D locations of corresponding features based on the principles of photogrammetry (Snavely, Seitz, & Szeliski, 2008; Westoby, Brasington, Glasser, Hambrey, & Reynolds, 2012).

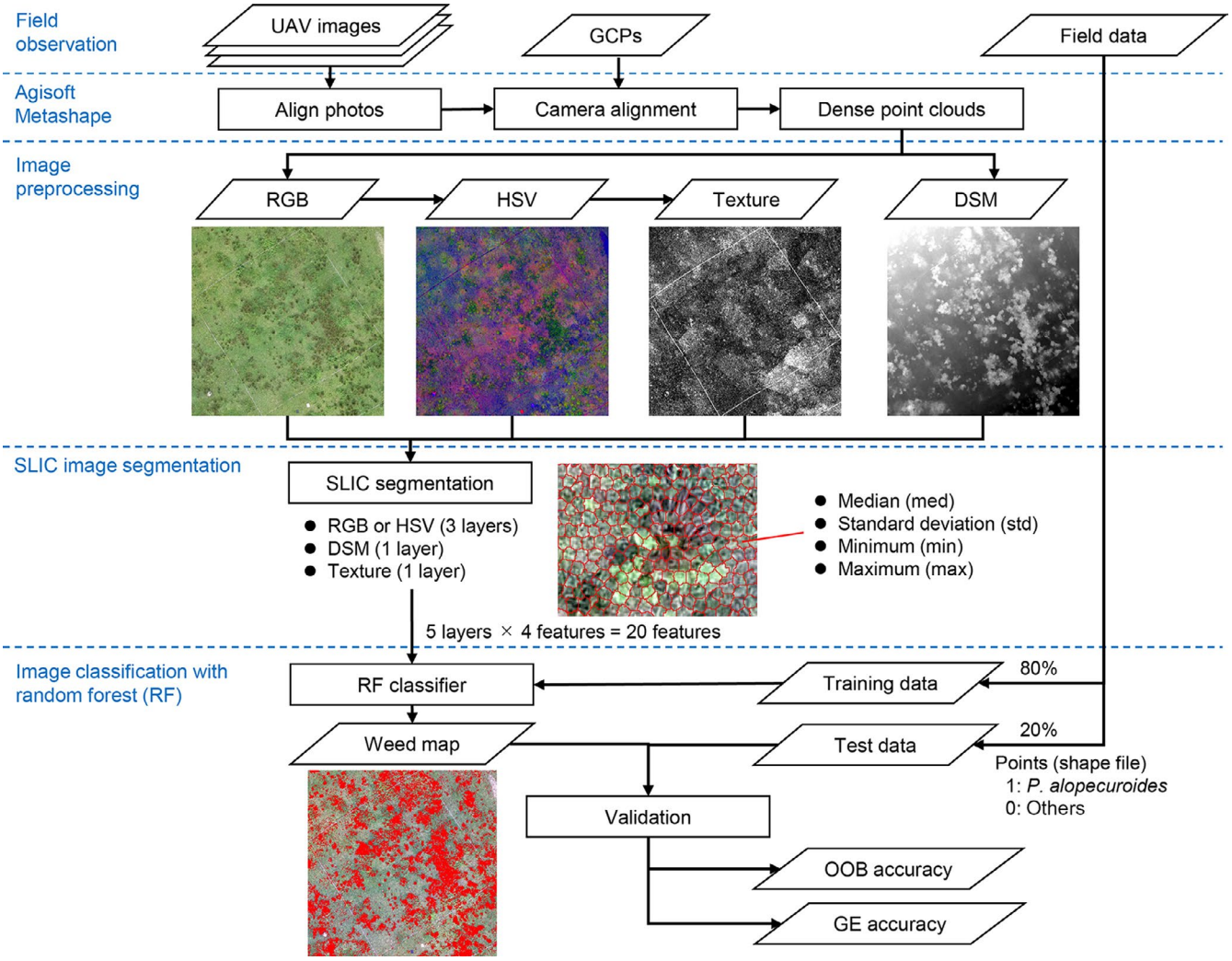

FIGURE 2 Schematic of image counting procedure

2.5 | HSV and Texture images

In HSV images, brightness (V) is unrelated to the color information of the images. The hue (H) represents the property of the color; saturation (S) represents the purity of the color, while V represents the shading of the color.

The layers of spatial texture information were created by applying a local variance filter (7 × 7 pixels) to UAV RGB band images (Zisi et al., 2018). Spatial texture refers to the visual effect caused by spatial variation in tonal quantity over relatively small areas (Anys & He, 1995). In the present study, higher discrimination ability of *P. alopecuroides* was observed in the G band (Figure 3); therefore, it was selected for use in image classification.

2.6 | SLIC superpixel image segmentation

Simple linear iterative clustering (SLIC) was initially introduced by (Achanta et al., 2010) and later extended to a zero parameter version, SLICO (Achanta et al., 2012). SLIC uses an adapted *k*-means clustering integrating color similarity and proximity in image pixels, which includes CIELAB (L^*, a^*, and b) color and their x and y coordinates.

In the present study, SLIC superpixel image segmentation was performed using the scikit-learn package (Pedregosa et al., 2011) in Python. We used the second version of SLIC (SLICO) with number of superpixels (k) = 10. It generates regular-shaped superpixels across the scene (Achanta et al., 2012), as shown in Figure 4.

Four statistical features, including median (med), standard deviation (std), minimum (min) and maximum (max) values, were extracted for each object from 5 layers (RGB or HSV + DSM + Texture). In total, 20 features (5 layers × 4 stats) were applied as input features in RF classification.

2.7 | RF classification

Random forest is an ensemble of numerous independent individual classification and regression tree (CART) (Breiman, 2001). The final output of RF is calculated based on the maximum votes from the number of trees (*ntree*). A more detailed overview and recent developments of RF in remote sensing can be found in Belgiu and Drăguţ (2016).

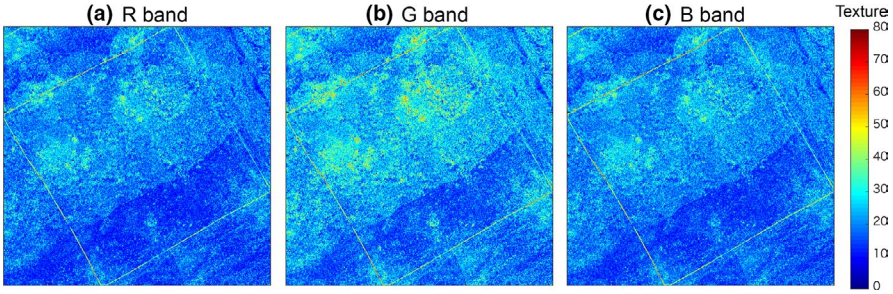

FIGURE 3 Texture images from R (a), G (b) and B (c) bands in plot A

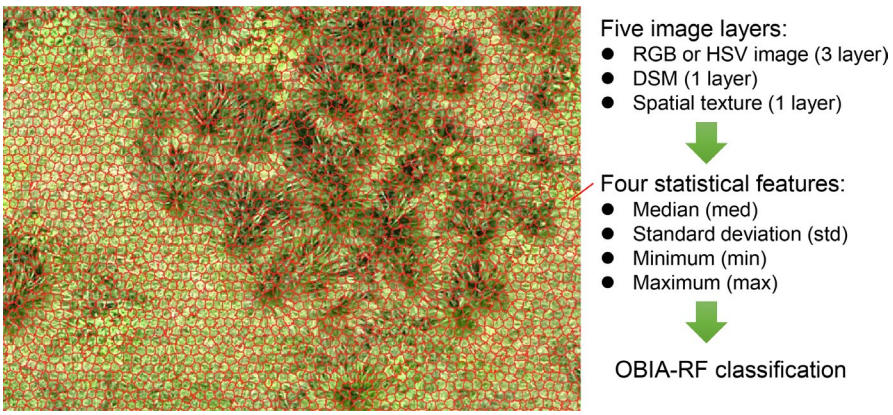

FIGURE 4 Simple linear iterative clustering (SLIC) applied to ortho-mosaic-red-green-blue image of plot A with 0.90 cm ground sampling distance (GSD) and initial clustering of 10 × 10 pixels (k = 10), and flow of input features extraction process

In the present study, RF classification was performed using the scikit-learn package (Pedregosa et al., 2011) in Python using 20 input features from OBIA (see Figure 4). Here, RF classification was performed with *ntree* = 5,000. Initially, the dataset was split into a training dataset (80%) for building a model and a test (20%) dataset for validating the accuracy of the model. Using the training dataset, the RF model built a set of trees that were created by selecting a subset through a bagging approach, while the remaining subset, called out of bag (OOB), was used for internal cross-validation. The OOB data are used to compute accuracies and error rates averaged over all predictions (Cutler et al., 2007) and estimate variable (feature) importance.

In RF classification, there are two methods for estimating the importance of each input features (predictor variables) in the model. One is the mean decrease in accuracy (MDA), which is calculated as the normalized difference between the OOB accuracy of the original observations and the OOB accuracy of randomly permuted features (variables) (Cutler et al., 2007; Mellor, Haywood, Stone, & Jones, 2013). Another feature importance measure is calculated by summing all the decreases in Gini impurity at each tree node split, normalized by the number of trees (Criminisi, 2011; Mellor et al., 2013). In the present study, we used Gini impurity to assess the importance of 20 input features.

2.8 | Classification accuracy

To compare the performance of OBIA-RF classifications, OOB accuracy and generalized error (GE) accuracy were used in the present study. The OOB accuracy was calculated using OOB error in the internal cross-validation process, which is defined as follows:

$$\text{OOB accuracy} = 1 - \text{OOB error} \quad (1)$$

where OOB error is the fraction of the number of incorrect classifications over number of OOB samples. The OOB can be used to assess how well the RF model performs (Belgiu & Drăguţ, 2016).

To assess the classification accuracy in the final model, GE accuracy was calculated as follows:

$$\text{GE accuracy} = 1 - \text{GE error} \quad (2)$$

where GE error is the fraction of the number of incorrect classifications between the observed and the predicted classification results from the final model.

3 | RESULTS

3.1 | Spatial resolution and covered area of image at different flight altitudes

In Figure 5, the spatial resolutions of mosaic RGB images at different flight heights (28, 56, 82 and 114 m) were compared visually. Spatial resolution and ground sampling distance (GSD) depend on the flight altitude, and they are the key factors influencing classification accuracy. In the present study, the spatial resolutions at 28, 56, 82 and 114 m flight altitude were 0.90, 1.82, 2.64 and 3.63 cm, respectively. The image with the highest spatial resolution (0.90 cm) revealed the GCP (30 × 30 cm) clearly in the center of the plot (Figure 5a), while the outline was unclear in the low-resolution image, at 3.63 cm (Figure 5d).

FIGURE 5 Visual comparison of spatial resolution in mosaic red-green-blue (RGB) images at different flight altitudes: (a) 28 m, (b) 56 m, (c) 82 m and (d) 114 m

3.2 | OBIA-RF classification results

Based on OOB accuracies, eight classifications were compared between plots A and B (Table 1): Eight models included two different color features (RGB, HSV) from UAV images captured at different flight altitudes (28, 56, 82 and 114 m). Excluding the RGB-based model in plot A, the OOB accuracies were the highest in the models with the highest spatial resolution image that was obtained using the UAV at a flight altitude of 28 m. Compared to the RGB-based model, the HSV color feature-based model had higher classification accuracy in both plot A and plot B. The highest OOB accuracy in plot A (0.966) and plot B (0.992) was achieved in the classification performed using HSV-based input features at a flight altitude of 28 m. To assess the classification ability, GE accuracy was computed by the HSV-based models applied to individual test dataset, indicating very high GE accuracy in plot A (0.962) and plot B (1.000), respectively.

TABLE 1 Out of bags (OOB) accuracy of object-based image analysis (OBIA) combined with random forest (RF) classifications using 20 features from unmanned aerial vehicle (UAV) images at four different flight altitudes

			OOB accuracy	
Features (median, std, max, min)	Flight altitude (m)	GSD (cm)	Plot A	Plot B
RGB + DSM + Texture	28	0.90	0.918	0.940
	56	1.82	0.922	0.927
	82	2.64	0.937	0.912
	114	3.63	0.885	0.813
HSV + DSM + Texture	28	0.90	0.966	0.992
	56	1.82	0.961	0.984
	82	2.64	0.950	0.958
	114	3.63	0.946	0.922

Abbreviations: DSM, digital surface model; GSD, ground sampling distance; HSV, hue-saturation-brightness; RGB, red-greed-blue.

3.3 | Important features

To assess the input features' contribution to classification accuracy, the importance of 20 features (5 layers × 4 statistical features within object) based on RF procedures are illustrated in Figure 6. In the RGB image-based OBIA-RF procedure (Figure 6a,b), the important features were different between plots A and B. In plot A, the three most important features were Rmed, Gmed and Bstd, and in plot B, the three most important features were Gmed, DSMstd and Tmax. The green band exhibited the most or second most importance, which was mainly because *P. alopecuroides* had a green color that was distinct from other vegetation.

In the HSV-based OBIA-RF procedure (Figure 6c,d), the four most important features were similar between plots A and B (Vmed, Vmax, Smed and Vmin). Compared to the RGB-based OBIA-RF results, the results of the DSM indicated lower importance. Texture features showed moderate importance in most of the OBIA-RF procedures. Overall, the G band and HSV were more important compared to all the other features. The results indicated that although the texture features could be contributed to increase classification precision of RF classifier, color features remain the most important features in *P. alopecuroides* discrimination. Particularly, V feature could be the most important feature in OBIA-RF model for discriminating *P. alopecuroides* plants.

3.4 | Spatial distribution map of *P. alopecuroides* plants

Figure 7 presents spatial distribution maps of predicted *P. alopecuroides* plants from the OBIA-RF model applied to HSV-UAV images at

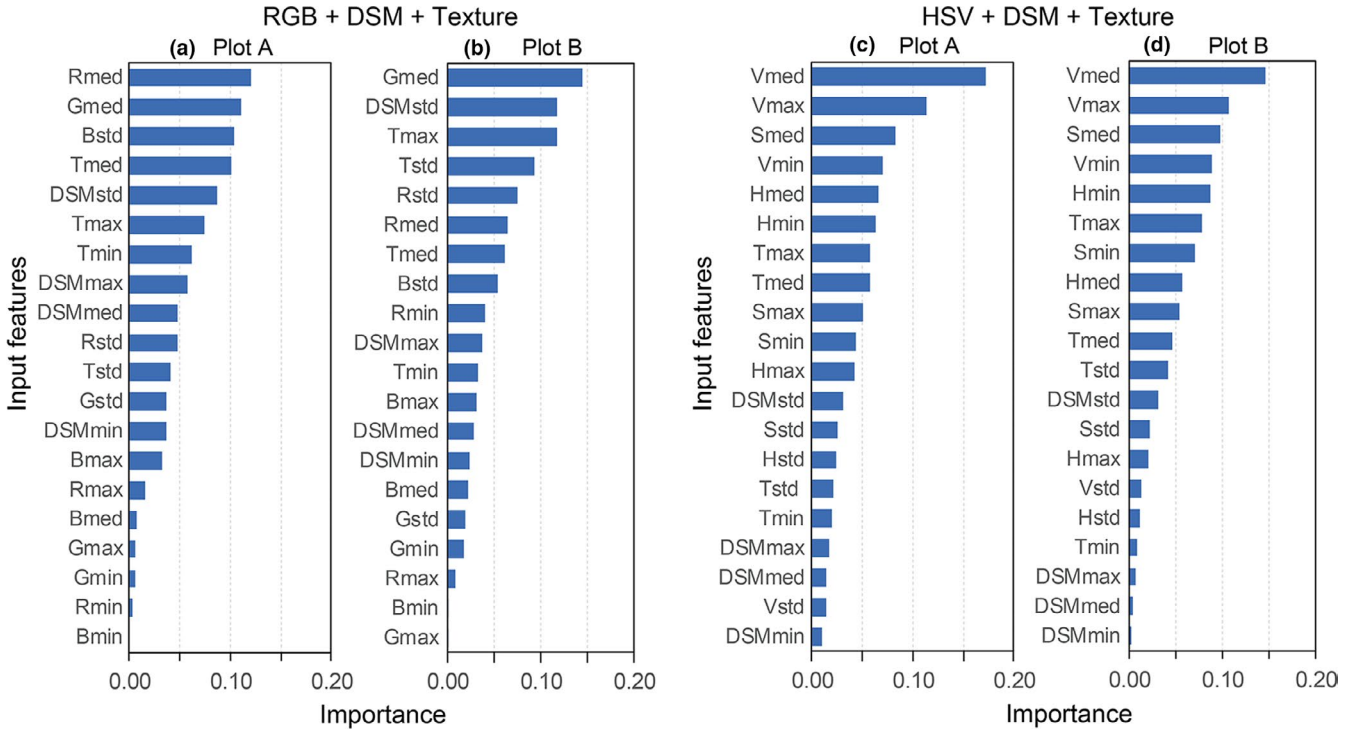

FIGURE 6 Importance of input features (red-green-blue [RGB] or hue-saturation-brightness [HSV] +digital surface model [DSM] +Texture) in plot A (a, c) and plot B (b, d)

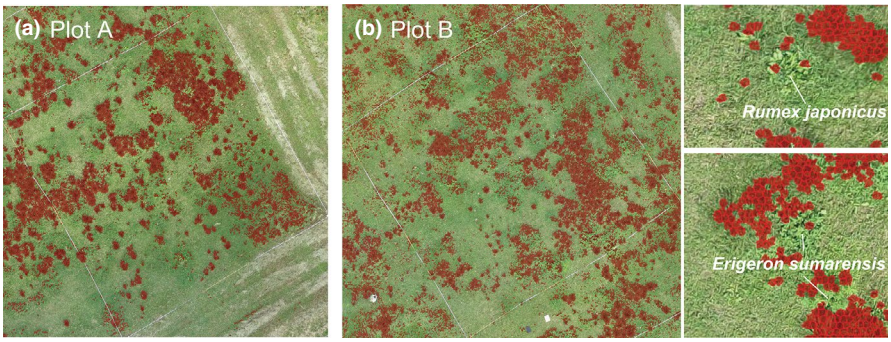

FIGURE 7 Spatial distribution maps of *P. alopecuroides* plants predicted from unmanned aerial vehicle (UAV) images using the object-based image analysis (OBIA) combined with random forest (RF) classifier in plot A (a) and plot B (b)

a flight altitude of 25 m. Even though there were several weeds such as *Rumex japonicus* and *Erigeron sumarensis* in addition to *P. alopecuroides*, the distribution of *P. alopecuroides* plants was accurately extracted from UAV image. The cover ratios of the *P. alopecuroides* plants in plot A and B were 30.3% and 23.7%, respectively. The *P. alopecuroides* plant distribution was not uniform. In plot A, which was located at the edge of a paddock with larger coverage area, and was considered to have been invaded earlier, *P. alopecuroides* formed large patches.

4 | DISCUSSION

In the present study, we applied OBIA on UAV images and integrated RF classifier to improve the classification accuracy when discriminating *P. alopecuroides* in pasture. Today, image segmentation in OBIA is a key step in UAV image information extraction and target detection (Dong, Wang, & Li, 2017). In addition, the RF algorithm is increasingly attracting attention in remote sensing research as a highly suitable tool for high-resolution image data classification (Ma, Cheng, Li, Liu, & Ma, 2015). By combining OBIA and RF, further improvements in classification could be obtained (Csillik, 2017; Yasuda, 2018).

In weed detection, the spatial resolution of the images and plant density influence classification accuracies (de Castro et al., 2018). Our UAV observations at different flight heights (28, 56, 82 and 114 m) obtained mosaic images with different spatial resolutions (0.90, 1.82, 2.64 and 3.63 cm). The UAV image with the highest spatial resolution achieved the best classification accuracies in both plots, excluding the RGB-based model in plot A (Table 1). For image discrimination, in general, the detection for smallest objects within an image requires at least four pixels (Hengl, 2006). Based on our field survey, the plant widths (diameter, cm) of individual *P. alopecuroides* plants ranged from 14 to 105 cm (n = 811) in both plots. Accordingly, if the discrimination of individual *P. alopecuroides* plants is the objective, the required pixel size should be less than approximately 3.5 cm (= 14 cm/4

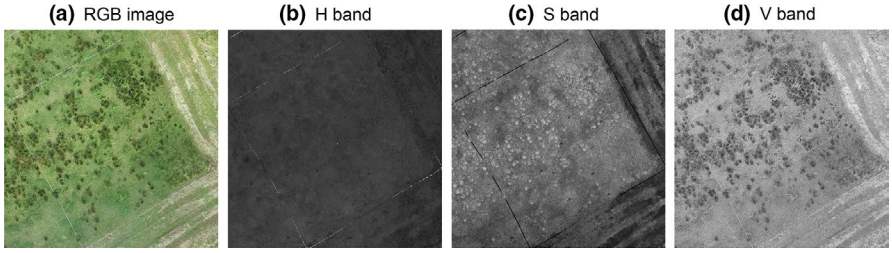

FIGURE 8 Red-green-blue (RGB) image (a) and H (b), S (c) and V (d) bands from hue-saturation-brightness (HSV) image

pixel). This corresponds to flight altitudes of 28, 56 and 82 m, and a flight altitude of 114 m (3.63 cm) would be not appropriate.

However, during the field observation, plant growth was considered to have peaked. If it was performed during an earlier growth stage, the required pixel size would have to be smaller due to the small sizes of the plants. For example, Peña et al. (2015) reported that 1 cm is the pixel size required for discriminating individual weed plants at the early growth stages in a sunflower field. They also argued that the pixel size of UAV images should be 5 cm or even greater for weed patch detection. In the present study, large patches were observed in plot A in the field survey and in the predicted map (Figure 7). This could be why the optimal classification accuracy was obtained using the RGB-based model using low spatial resolution UAV images (2.64 cm) in plot A.

In many cases where weed color is similar to that of grass or a crop, color alone is potentially inadequate for distinguishing weed pixels from pixels of other vegetation accurately (Hamuda, Mc Ginley, Glavin, & Jones, 2017). In the present study, we compared two color space features (RGB or HSV) with DSM and texture for developing models using UAV images captured at different flight altitudes. In addition, in each image layer, four statistical features were extracted from each object, and a total of 20 features (5 layers × 4 statistical features) were used in the RF classifications. Overall, the optimal classification accuracy was obtained in the HSV-based model using the highest spatial resolution UAV image (OOB accuracy = 0.992, GE accuracy = 1.000). Compared to the classification accuracy in our previous study (accuracy = 0.803 with image captured at a 56-m flight altitude) that adopted a pixel-based approach (Yuba et al., 2020), the OBIA-RF method improved the classification accuracy in the present study considerably. The result is consistent with previous findings indicating that RF is a suitable approach for high-resolution UAV data classification (Ma et al., 2015) and that the combination of OBIA with auxiliary information layers improves classification accuracy (Csillik, 2017).

Among the input features, the HSV feature was considered the most important variable influencing the discrimination of *P. alopecuroides* plants (Figure 6). The HSV color space is more aligned with human color perception (Sobottka & Pitas, 1996) and robust to illumination variation (Chaves-González, Vega-Rodríguez, Gómez-Pulido, & Sánchez-Pérez, 2010). Earlier studies compared several color spaces to determine the most optimal ones for image segmentation (Liu, Mu, Wang, & Yan, 2012; Panneton & Brouillard, 2009; Philipp & Rath, 2002); however, the recommended features differed depending on targeted plants. To assess the individual H, S and V features, Figure 8 illustrates the original RGB image in plot A, and the individual H, S and V bands from the HSV image. In the V band image, *P. alopecuroides* plants exhibited lower V intensity (brightness) than other vegetation and soil surfaces because on the field observation date, the *P. alopecuroides* plants had passed the heading stage, and the ears were black in color (Yuba et al., 2020).

Our results confirmed that *P. alopecuroides* plant could be mapped with good classification accuracy using UAV remote sensing data based on an OBIA-RF approach. However, we note that the results were based on a single UAV flight in the heading stage and considering *P. alopecuroides* ears are black. We did not investigate other growing seasons, especially in earlier growing season when the *P. alopecuroides* plant has none of ears and shows green like other grasses. As the plants are growing and their widths and colors are varied throughout the growing season, it would be necessary to evaluate the appropriate UAV observation time and other input features. Nevertheless, the OBIA-RF approach improved accuracy for discriminating the *P. alopecuroides* plant at heading stage and the automation of OBIA-RF processing could facilitate timely weed detection (de Castro et al., 2018), which could aid farmers in weed control to improve productivity in grazed pasture.

5 | CONCLUSIONS

The present study applied an OBIA-RF algorithm on UAV images to detect and map *P. alopecuroides* plants at heading stage in a pasture. We compared the classification accuracies of UAV images captured at different flight heights (28, 56, 82 and 114 m), and using two color spaces for input features with auxiliary information layers (DSM and spatial texture). Our results confirmed that the integration of RF and OBIA with auxiliary information layers enhanced classification accuracy. UAV images at different flight altitude suggest that the lowest altitude of 28 m could provide images with a spatial resolution (0.9 cm) suitable for the detection of *P. alopecuroides* plants. For color features information, superior results were observed in the HSV-based OBIA-RF models compared to the results of the RGB-based models. The V feature influenced classification the most because *P. alopecuroides* ears are black. Overall, the optimal classification accuracy was obtained by the model using HSV color features and the UAV dataset with the highest spatial resolution (OOB accuracy = 0.992, GE accuracy = 1.000). In the future, the automation of OBIA-RF could facilitate real-time weed detection in pasture.

ACKNOWLEDGMENTS

We express our sincere thanks to all the staff of the Setouchi Field Science Center, Saijo Station, Hiroshima University, for their assistance during the field experiments. We would like to thank Editage (www.editage.com) for English language editing.

ORCID

Kensuke Kawamura https://orcid.org/0000-0002-2824-1266
Jihyun Lim https://orcid.org/0000-0003-0452-4218

REFERENCES

Achanta, R., Shaji, A., Smith, K., Lucchi, A., Fua, P., & Susstrunk, S. (2010). SLIC superpixels. *EPFL Technical Report*, *149300*, 15. https://doi.org/10.1109/TPAMI.2012.120

Achanta, R., Shaji, A., Smith, K., Lucchi, A., Fua, P., & Süsstrunk, S. (2012). SLIC superpixels compared to state-of-the-art superpixel methods. *IEEE Transactions on Pattern Analysis and Machine Intelligence*, *34*(11), 2274–2281. https://doi.org/10.1109/TPAMI.2012.120

Anys, H., & He, D. C. (1995). Evaluation of textural and multipolarization radar features for crop classification. *IEEE Transactions on Geoscience and Remote Sensing*, *33*(5), 1170–1181. https://doi.org/10.1109/36.469481

Beaulieu, J. M., & Goldberg, M. (1989). Hierarchy in picture segmentation: A stepwise optimization approach. *IEEE Transactions on Pattern Analysis and Machine Intelligence*, *11*(2), 150–163. https://doi.org/10.1109/34.16711

Belgiu, M., & Drăguţ, L. (2016). Random forest in remote sensing: A review of applications and future directions. *ISPRS Journal of Photogrammetry and Remote Sensing*, *114*, 24–31. https://doi.org/10.1016/j.isprsjprs.2016.01.011 https://doi.org/

Blaschke, T., Hay, G. J., Kelly, M., Lang, S., Hofmann, P., Addink, E., … Tiede, D. (2014). Geographic object-based image analysis – Towards a new paradigm. *ISPRS Journal of Photogrammetry and Remote Sensing*, *87*, 180–191. https://doi.org/10.1016/j.isprsjprs.2013.09.014

Breiman, L. (2001). Random forests. *Machine Learning*, *45*(1), 5–32. https://doi.org/10.1023/A:1010933404324

Chaves-González, J. M., Vega-Rodríguez, M. A., Gómez-Pulido, J. A., & Sánchez-Pérez, J. M. (2010). Detecting skin in face recognition systems: A colour spaces study. *Digital Signal Processing: A Review Journal*, *20*(3), 806–823. https://doi.org/10.1016/j.dsp.2009.10.008

Cheng, M. M., Mitra, N. J., Huang, X., Torr, P. H. S., & Hu, S. M. (2015). Global contrast based salient region detection. *IEEE Transactions on Pattern Analysis and Machine Intelligence*, *37*(3), 569–582. https://doi.org/10.1109/TPAMI.2014.2345401

Comaniciu, D., & Meer, P. (2002). Mean shift: A robust approach toward feature space analysis. *IEEE Transactions on Pattern Analysis and Machine Intelligence*, *24*(5), 603–619. https://doi.org/10.1109/34.1000236

Criminisi, A. (2011). Decision forests: A unified framework for classification, regression, density estimation, manifold learning and semi-supervised learning. *Foundations and Trends® in Computer Graphics and Vision*, *7*(2–3), 81–227. https://doi.org/10.1561/0600000035

Csillik, O. (2017). Fast segmentation and classification of very high resolution remote sensing data using SLIC superpixels. *Remote Sensing*, *9*(3), 243. https://doi.org/10.3390/rs9030243

Cutler, D. R., Edwards, T. C., Beard, K. H., Cutler, A., Hess, K. T., Gibson, J., & Lawler, J. J. (2007). Random forests for classification in ecology. *Ecology*, *88*(11), 2783–2792. https://doi.org/10.1890/07-0539.1

de Castro, A. I., Torres-Sánchez, J., Peña, J. M., Jiménez-Brenes, F. M., Csillik, O., & López-Granados, F. (2018). An automatic random forest-OBIA algorithm for early weed mapping between and within crop rows using UAV imagery. *Remote Sensing*, *10*(2), 285. https://doi.org/10.3390/rs10020285

Dong, Z., Wang, M., & Li, D. (2017). A high resolution remote sensing image segmentation method by combining superpixels with minimum spanning tree. *Acta Geodaetica Et Cartographica Sinica*, *46*(6), 734–742. https://doi.org/10.11947/j.AGCS.2017.20160514

Felzenszwalb, P. F., & Huttenlocher, D. P. (2004). Efficient graph-based image segmentation. *International Journal of Computer Vision*, *59*(2), 167–181. https://doi.org/10.1023/B:VISI.0000022288.19776.77

Gebhardt, S., & Kühbauch, W. (2007). A new algorithm for automatic *Rumex obtusifolius* detection in digital images using colour and texture features and the influence of image resolution. *Precision Agriculture*, *8*(1), 1–13. https://doi.org/10.1007/s11119-006-9024-7

Ghanizadeh, H., & Harrington, K. C. (2019). Weed management in New Zealand pasture. *Agronomy*, *9*(8), 448. https://doi.org/10.3390/agronomy9080448

Hamuda, E., Mc Ginley, B., Glavin, M., & Jones, E. (2017). Automatic crop detection under field conditions using the HSV colour space and morphological operations. *Computers and Electronics in Agriculture*, *133*, 97–107. https://doi.org/10.1016/j.compag.2016.11.021

Haris, K., Efstratiadis, S. N., & Maglaveras, N. (1998). Watershed-based image segmentation with fast region merging. In *Proceedings 1998 International Conference on Image Processing*. ICIP98 (Cat. No.98CB36269) (Vol. *3*, pp. 338–342). IEEE Comput. Soc.

Hayashi, H. (2002). Control of Chikarashiba by goat grazing: Verification of optimum grazing pressure. *Japanese Journal of Grassland Science*, *48*(Ex), 88–89. (In Japanese) https://doi.org/10.14941/grass.48.88

Hengl, T. (2006). Finding the right pixel size. *Computers & Geosciences*, *32*(9), 1283–1298. https://doi.org/10.1016/j.cageo.2005.11.008

Ide, Y., Koyama, N., Takahashi, Y., Kobayashi, H., & Fukuda, E. (2006). Temporal changes in the number of seeds attached to grazing cattle. *Japanese Journal of Grassland Science*, *52*(Ex), 312–313. (In Japanese)

Lim, J., Kawamura, K., Lee, H.-J., Yoshitoshi, R., Kurokawa, Y., Tsumiyama, Y., & Watanabe, N. (2015). Evaluating a hand-held crop-measuring device for estimating the herbage biomass, leaf area index and crude protein content in an Italian ryegrass field. *Grassland Science*, *61*(2), 101–108. https://doi.org/10.1111/grs.12083

Liu, Y., Mu, X., Wang, H., & Yan, G. (2012). A novel method for extracting green fractional vegetation cover from digital images. *Journal of Vegetation Science*, *23*(3), 406–418. https://doi.org/10.1111/j.1654-1103.2011.01373.x

Llewellyn, R. S., Lindner, R. K., Pannell, D. J., & Powles, S. B. (2004). Grain grower perceptions and use of integrated weed management. *Australian Journal of Experimental Agriculture*, *44*, 993–1001. https/doi.org/10.1071/EA03115.

Ma, L., Cheng, L., Li, M., Liu, Y., & Ma, X. (2015). Training set size, scale, and features in geographic object-based image analysis of very high resolution unmanned aerial vehicle imagery. *ISPRS Journal of Photogrammetry and Remote Sensing*, *102*, 14–27. https://doi.org/10.1016/j.isprsjprs.2014.12.026

Mellor, A., Haywood, A., Stone, C., & Jones, S. (2013). The performance of random forests in an operational setting for large area sclerophyll forest classification. *Remote Sensing*, *5*(6), 2838–2856. https://doi.org/10.3390/rs5062838

Panneton, B., & Brouillard, M. (2009). Colour representation methods for segmentation of vegetation in photographs. *Biosystems Engineering*, *102*(4), 365–378. https://doi.org/10.1016/j.biosystemseng.2009.01.003

Pedregosa, F., Varoquaux, G., Gramfort, A., Michel, V., Thirion, B., Grisel, O., … Duchesnay, É. (2011). Scikit-learn: Machine learning in Python. *Journal of Machine Learning Research*, *12*, 2825–2830.

Peña, J. M., Torres-Sánchez, J., de Castro, A. I., Kelly, M., & López-Granados, F. (2013). Weed mapping in early-season maize fields using object-based analysis of unmanned aerial vehicle (UAV) images. *PLoS ONE*, *8*(10), e77151. https://doi.org/10.1371/journal.pone.0077151

Peña, J. M., Torres-Sánchez, J., Serrano-Pérez, A., de Castro, A. I., & López-Granados, F. (2015). Quantifying efficacy and limits of unmanned aerial vehicle (UAV) technology for weed seedling detection as affected by sensor resolution. *Sensors*, *15*(3), 5609–5626. https://doi.org/10.3390/s150305609

Philipp, I., & Rath, T. (2002). Improving plant discrimination in image processing by use of different colour space transformations. *Computers and Electronics in Agriculture*, *35*(1), 1–15. https://doi.org/10.1016/S0168-1699(02)00050-9

Ren, X., & Malik, J. (2003). Learning a classification model for segmentation. In *Proceedings of the IEEE International Conference on Computer Vision* (Vol. *1*, pp. 10–17). IEEE.

Rodriguez-Galiano, V. F., Ghimire, B., Rogan, J., Chica-Olmo, M., & Rigol-Sanchez, J. P. (2012). An assessment of the effectiveness of a random forest classifier for land-cover classification. *ISPRS Journal of Photogrammetry and Remote Sensing*, *67*(1), 93–104. https://doi.org/10.1016/j.isprsjprs.2011.11.002

Sakai, H. (1978). Weeds of sown grassland in Japan. *Journal of Weed Science and Technology*, *23*(4), 151–159. (In Japanese). https://doi.org/10.3719/weed.23.151

Shaw, D. R. (2005). Remote sensing and site-specific weed management. *Frontiers in Ecology and the Environment*, *3*(10), 526–532. https://doi.org/10.1890/1540-9295(2005)003[0526:RSASWM]2.0.CO;2

Shi, J., & Malik, J. (2000). Normalized cuts and image segmentation. *IEEE Transactions on Pattern Analysis and Machine Intelligence*, *22*(8), 888–905. https://doi.org/10.1109/34.868688

Snavely, N., Seitz, S. M., & Szeliski, R. (2008). Modeling the world from Internet photo collections. *International Journal of Computer Vision*, *80*(2), 189–210. https://doi.org/10.1007/s11263-007-0107-3

Sobottka, K., & Pitas, I. (1996). Face localization and facial feature extraction based on shape and color information. In *IEEE International Conference on Image Processing* (Vol. *3*, pp. 483–486). IEEE.

Stutz, D., Hermans, A., & Leibe, B. (2018). Superpixels: An evaluation of the state-of-the-art. *Computer Vision and Image Understanding*, *166*, 1–27. https://doi.org/10.1016/j.cviu.2017.03.007

Takahashi, S., & Takahashi, S. (1999). Seed breeding and productivity of Chikarashiba under cutting conditions assuming different foraging pressures. *Journal of Japanese Society of Grassland Science*, *45*, 66–67. (In Japanese). https://doi.org/10.14941/grass.45.66

Takahashi, S., Takahashi, S., Shibayama, M., & Imura, T. (1999). Grazing intensity and herbage biomass change model: Model experiment to control Chikarashiba. *Journal of Japanese Society of Grassland Science*, *45*, 2–3. (In Japanese) https://doi.org/10.14941/grass.45.2

Tamouridou, A. A., Alexandridis, T. K., Pantazi, X. E., Lagopodi, A. L., Kashefi, J., & Moshou, D. (2017). Evaluation of UAV imagery for mapping *Silybum marianum* weed patches. *International Journal of Remote Sensing*, *38*(8–10), 2246–2259. https://doi.org/10.1080/01431161.2016.1252475

Tremeau, A., & Colantoni, P. (2000). Regions adjacency graph applied to color image segmentation. *IEEE Transactions on Image Processing*, *9*(4), 735–744. https://doi.org/10.1109/83.841950

Wang, M., Dong, Z., Cheng, Y., & Li, D. (2018). Optimal segmentation of high-resolution remote sensing image by combining superpixels with the minimum spanning tree. *IEEE Transactions on Geoscience and Remote Sensing*, *56*(1), 228–238. https://doi.org/10.1109/TGRS.2017.2745507

Westoby, M. J., Brasington, J., Glasser, N. F., Hambrey, M. J., & Reynolds, J. M. (2012). 'Structure-from-Motion' photogrammetry: A low-cost, effective tool for geoscience applications. *Geomorphology*, *179*, 300–314. https://doi.org/10.1016/j.geomorph.2012.08.021

Yasuda, T. (2018). Semi-natural grassland vegetation mapping utilizing unmanned aerial vehicles and image analysis. *Japanese Journal of Grassland Science*, *64*(1), 43–47. (In Japanese) https://doi.org/10.14941/grass.64.43

Yokoyama, R., Shirasawa, M., & Pike, R. J. (2002). Visualizing topography by openness: A new application of image processing to digital elevation models. *Photogrammetric Engineering and Remote Sensing*, *68*(3), 257–265.

Yuba, N., Kawamura, K., Yasuda, T., Lim, J., Yoshitoshi, R., Kurokawa, Y., & Maeda, T. (2020). Counting of *Pennisetum alopecuroides* at heading stage in a grazed pasture using images from an unmanned aerial vehicle. *Grassland Science*, https://doi.org/10.1111/grs.12277

Zisi, T., Alexandridis, T. K., Kaplanis, S., Navrozidis, I., Tamouridou, A. A., Lagopodi, A., … Polychronos, V. (2018). Incorporating surface elevation information in UAV multispectral images for mapping weed patches. *Journal of Imaging*, *4*(11), 132. https://doi.org/10.3390/jimaging4110132

How to cite this article: Yuba N, Kawamura K, Yasuda T, et al. Discriminating *Pennisetum alopecuoides* plants in a grazed pasture from unmanned aerial vehicles using object-based image analysis and random forest classifier. *Grassl Sci*. 2021;67:73–82. https://doi.org/10.1111/grs.12288